Looking for BSM physics using top-quark polarization and decay-lepton kinematic asymmetries

Rohini M. Godbole,[1] Gaurav Mendiratta,[1] and Saurabh D. Rindani[2]

[1]*Centre for High Energy Physics, Indian Institute of Science, Bangalore 560 012, India*
[2]*Theoretical Physics Division, Physical Research Laboratory, Navrangpura, Ahmedabad 380 009, India*

(Received 13 July 2015; published 9 November 2015)

We explore beyond-standard-model (BSM) physics signatures in the $l+$jets channel of the $t\bar{t}$ pair production process at the Tevatron and the LHC. We study the effects of BSM physics scenarios on the top-quark polarization and on the kinematics of the decay leptons. To this end, we construct asymmetries using the lepton energy and angular distributions. Further, we find their correlations with the top polarization, net charge asymmetry and top forward-backward asymmetry. We show that when used together, these observables can help discriminate effectively between SM and different BSM scenarios, which can lead to varying degrees of top polarization at the Tevatron as well as the LHC. We use two types of colored mediator models to demonstrate the effectiveness of proposed observables, an s-channel axigluon and a u-channel diquark.

DOI: 10.1103/PhysRevD.92.094013 PACS numbers: 14.65.Ha, 13.88.+e, 13.90.+i

I. INTRODUCTION

Most experimental observations at particle accelerators fit the standard model (SM) very well. However, there are some major puzzles to be solved. One needs to have physics beyond the standard model (BSM) to explain the presence of dark matter, to explain quantitatively the observed baryon asymmetry of the Universe, and to explain the puzzle of dark energy. Looking for signs of BSM, one finds that most of the terrestrial experimental observations that are in tension with the SM results are in the properties of third-generation fermions. For example, $B \to \tau\nu$ [1], $h \to \mu\tau$ [2] and $b\bar{b}$ forward-backward asymmetry (AFB) at LEP and Tevatron [3–5] show such deviations. One of these longstanding puzzles is the top-quark AFB measured by the D0 and CDF detectors at the Tevatron collider in 2008 [6,7]. These observations by two independent collaborations were updated with full data from the Tevatron and were consistent with each other and in tension with the SM calculations until 2015. Recent experimental results from D0 [8] and theoretical calculations [9] point towards the possibility that the anomalous nature of these observations may be a statistical phenomenon.

Due to its large mass, which is close to the electroweak scale, and the implied connection with electroweak symmetry breaking, the top quark is an important laboratory for various BSM searches at colliders. In fact, various proposals put forward to solve the different theoretical problems of the SM often involve modifications in the top sector. Various extensions to the SM have also been proposed inspired by the possibly anomalous value of measured top AFB at the Tevatron. These BSM proposals involve explanation of the AFB in terms of processes involving (a) s-channel resonances like the axigluon, KK gluon, and coloron [10–18], or (b) t-channel exchange of particles with different spins and SM charges like the Z', diquarks, etc. [14,16,17,19–25]. The effective operator approach has also been used in this context [26–28]. Measurements of other related observables such as lepton angular asymmetries and $t\bar{t}$ invariant mass dependence of the top-quark AFB are also compatible with the hypothesis of a heavy BSM particle, see for example Refs. [29,30].

In this study, we will focus on the lepton + jets final state ($p\bar{p}/pp \to t\bar{t} \to b\nu l\bar{t}$) of the $t\bar{t}$ pair production process. This channel has a larger cross section as compared to the dilepton + jets channel, and it has a much smaller background compared to the all-jets channel. For lighter quarks, hadronization smears the information available about their spin and polarization. The mass of the top quark is large enough that it decays into its daughter particles before strong interactions can initiate the hadronization process. Hence, top-quark polarization leaves a memory in the kinematic distribution of the decay products and can be tracked [31,32]. We study the correlations between various kinematic asymmetries and polarization to distinguish between different sources of these asymmetries within an s-channel (axigluon) and a t-channel (diquark) extension of the SM. For the Tevatron, the top pair production process is dominated by $q\bar{q}$ collisions, and at the LHC, it is dominated by gg collisions, which means that new physics can manifest differently at the two colliders.

A wide variety of observables have been studied in the literature to explore the top sector as a BSM portal [11,16,23,33–37]. A brief review of some of these observables which have been experimentally measured and are relevant to this work is presented in Sec. II. In Secs. III and IV we describe the flavor-nonuniversal axigluon and diquark models which we use as templates for our analysis. Constraints on these models from the top pair production cross section and forward-backward asymmetry at Tevatron; and from charge asymmetry, top-quark pair production, and dijet and four-jet production cross sections at LHC are

discussed in Sec. V. In Sec. VI we construct the asymmetries which we use to explore the BSM models. In Sec. VII we present the correlations between various asymmetries and discuss the role of top-quark polarization and kinematics in discerning the various regions of parameter space of the BSM models. We contrast our results for the axigluon and diquark models, and the resulting conclusions can be generalized to other new physics scenarios. Our results are presented for the Tevatron $\sqrt{s} = 1.96$ TeV and the LHC $\sqrt{s} = 7$ TeV, 13 TeV. We discuss the effects of transverse polarization coming from the off-diagonal terms in the top-quark density matrix in Sec. VIII and then conclude in Sec. IX.

II. STATUS OF EXPERIMENTAL RESULTS

We begin by summarizing some of the experimental results from the LHC and the Tevatron concerning the top quark and compare them with the corresponding SM calculations from the literature.

The measured $t\bar{t}$ production cross section for the Tevatron at $\sqrt{s} = 1.96$ TeV is $\sigma^{\text{Tevatron}}_{p\bar{p}\to t\bar{t}} = 7.60 \pm 0.41$ pb [38], and that for the LHC at $\sqrt{s} = 7$ TeV is $\sigma^{\text{LHC}}_{pp\to t\bar{t}} = 173.30 \pm 10.10$ pb [39,40]. These agree with the calculated SM NNLO cross sections, $\sigma^{\text{Tevatron}}_{p\bar{p}\to t\bar{t}} = 7.16^{+0.54}_{-0.50}$ pb [41] for the Tevatron and $\sigma^{\text{LHC7 TeV}}_{pp\to t\bar{t}} = 177.30 \pm 10.63$ pb [42] for the LHC, within 1σ. The uncertainties coming from the top-quark mass dependence of the $t\bar{t}$ cross section [43] have been included in the given LHC cross sections. In the calculations in following sections, we use a common K factor for the BSM + SM to estimate the NNLO total cross section. For the Tevatron, the K factor is $K_{\text{Tevatron}} = 1.39^{+0.10}_{-0.10}$ [44]. The K factor for the LHC is calculated using the NNLO cross section cited above and the LO cross section calculated using CTEQ6l parton distribution functions (PDFs) with factorization scale $Q = 2m_t$. The errors in the K factors represent PDF uncertainties, scale dependence and statistical errors in the NNLO cross section. For the LHC with $\sqrt{s} = 7$ TeV, $K_{\text{LHC7}} = 2.20^{+0.14}_{-0.15}$.

The cross sections impose a constraint on any new particle to have small couplings with the top quark and/or have a sufficiently high mass. It is interesting to note that we can still find a range of couplings of the BSM large enough to explain the measured anomalous top-quark and lepton asymmetries reported at the Tevatron and remain compatible with the measurements at the LHC. The AFB of the top quark in the $t\bar{t}$ center-of-mass (CM) frame is defined as

$$A_{\text{Forward Backward}} = \frac{N_F(y_t - y_{\bar{t}} > 0) - N_B(y_t - y_{\bar{t}} < 0)}{N_F(y_t - y_{\bar{t}} > 0) + N_B(y_t - y_{\bar{t}} < 0)}, \tag{1}$$

$$= \frac{N(\cos\theta_t > 0) - N(\cos\theta_t < 0)}{N(\cos\theta_t > 0) + N(\cos\theta_t < 0)}, \tag{2}$$

where y_t, $y_{\bar{t}}$ are, respectively, the rapidities of the t and the $\bar{t}$; and θ_t and $\theta_{\bar{t}}$ are their respective polar angles measured with respect to the beam direction.

The CDF measurement of the $t\bar{t}$ CM frame AFB with the full data set is $A^{t\bar{t}}_{FB} = 0.164 \pm 0.045$ [45]. The corresponding SM result is 0 at tree level in QCD. At NLO in QCD, the value predicted is $0.0589^{+0.0270}_{-0.0140}$ (the errors only represent scale variation), which upon including NLO electroweak corrections becomes $0.0734^{+0.0068}_{-0.0058}$ [46]. Recently, AFB has been calculated at NNLO to be $0.0749^{+0.0049}_{-0.0086}$ in pure QCD and 0.095 ± 0.007 including EW corrections [46] and including effective N^3LO QCD, $A^{t\bar{t},\text{SM}}_{\text{FB}} = 0.100 \pm 0.006$ [9]. D0 has come out recently with a measurement $A_{\text{FB}} = 0.106 \pm 0.03$ [8] which agrees with the theoretical results. However, for the purpose of this study, we use the CDF measurement which is still in tension with the SM and with the D0 measurement.

Since the LHC is a pp collider, its symmetric initial state makes the forward and backward regions trivially symmetric. For the LHC, instead of top-quark AFB, a charge asymmetry (AC) is defined in the lab frame as

$$A_C = \frac{N(\Delta|y_t| > 0) - N(\Delta|y_t| < 0)}{N(\Delta|y_t| > 0) + N(\Delta|y_t| < 0)}, \tag{3}$$

where $\Delta|y_t| = |y_t| - |y_{\bar{t}}|$. The AC at the LHC is much smaller than the AFB at the Tevatron both in the case of the SM and of the BSM models aimed at explaining the Tevatron's anomalous AFB. The measured value of AC with a CMS and ATLAS combination is $A_c = 0.005 \pm 0.009$ [47]. The theoretical results for the SM values of the AC [48] (QED + EW + NLO QCD) are given in Table I for different energies at the LHC.

Measurements have also been made for a number of other observables, including $M_{t\bar{t}}$, rapidity-dependent top AFB [45], lepton and dilepton asymmetries [49,50], some of which show a deviation from the standard model [35] of 1σ–3σ. Some CDF results are shown in Table II, and D0 results [50] are shown in Table III.

$t\bar{t}$ spin correlations have been measured using decay particle double distributions in polar and azimuthal angles at the Tevatron [51,52] and the LHC [53,54]. The polarization of the top quark, as defined in Eq. (12), has also been observed at CMS for the LHC 7 TeV run to be 0.01 ± 0.04 [54] compared to the corresponding SM prediction from

TABLE I. Charge asymmetry in the lab frame at the LHC, as defined in Eq. (3).

$\sqrt{s}$ (TeV)	A_C
7	0.0115(6)
12	0.0068(3)
13 (from fit; see Appendix A)	0.0063
14	0.0059(3)

TABLE II. CDF lepton and $M_{t\bar{t}}$ dependent top-level asymmetries [35,45,49].

Asymmetry	Experimental value	SM calculation
$A_{\mathrm{FB}}^{l}(\mathrm{or}\, A_{\theta_l})$	$0.090^{+0.028}_{-0.026}$	0.038 ± 0.003
$A_{t\bar{t}\_\mathrm{FB}}^{M_{t\bar{t}}>450\ \mathrm{GeV}}$	$0.295 \pm 0.058 \pm 0.031$	0.100 ± 0.030
$A_{t\bar{t}\_\mathrm{FB}}^{M_{t\bar{t}}<450\ \mathrm{GeV}}$	$0.084 \pm 0.046 \pm 0.026$	0.047 ± 0.014
$A_{\mathrm{FB}}^{l^+l^-}$	$0.094 \pm 0.024^{+0.022}_{-0.017}$	0.036 ± 0.002

TABLE III. D0 lepton asymmetries [50].

Asymmetry	Experimental value	SM calculation
$A_{\mathrm{FB}}^{l}(\mathrm{or}\, A_{\theta_l})$ (extrapolated)	0.047 ± 0.027	0.038 ± 0.003
$A_{\mathrm{FB}}^{l}(\lvert y_l\rvert < 1.5)$	$0.042^{+0.029}_{-0.030}$	0.02

MC@NLO [55] 0.000 ± 0.002. The ATLAS Collaboration also observed the polarization at 7 TeV beam energy, assuming a CP-conserving $t\bar{t}$ production and decay process, to be 0.035 ± 0.040 [56], in agreement with the SM prediction.

III. FLAVOR-NONUNIVERSAL AXIGLUON MODEL

An axigluon is a massive, colored ($SU(3)_c$ adj) vector boson. Models of axigluons which have only axial couplings with the quarks have been suggested in the literature in many GUT-like theories as chiral extensions of the QCD [57,58]. The contribution to AFB for such a particle was studied even before the possible anomalous AFB was observed at the Tevatron in 2008 [10]. For this flavor-universal, axially interacting massive gluon with coupling g_s, the top-quark AFB becomes negative for masses above $m_A \sim 500$ GeV. Upon the observation of a positive AFB by Tevatron in 2008, this model was found to be incompatible in the mass parameter regions allowed by the dijet constraints from Tevatron. The AFB turns back positive if the assumption of universality of the interaction of axigluons with the quark families is dropped [12]. In our study here, we have used a more general, flavor-nonuniversal axigluon with both axial-vector and vector couplings [13]. This model is obtained by breaking a larger symmetry group of $SU(3)_A \times SU(3)_B$ to leave an unbroken QCD color group $SU(3)_C$ and a massive gauge boson, the axigluon. The axial-vector coupling of the axigluon to the first- and second-generation quarks is the negative of that for the third generation, and the vector couplings are the same for all three generations. The couplings of the axigluon with quarks are described by the Lagrangian

$$\mathcal{L} = \bar{\psi}\gamma^{\mu}T^{a}(g_V + g_A\gamma^5)\psi A_{\mu}^{a}, \tag{4}$$

where T^a are the Gell-Mann matrices. The couplings are parametrized by $g_V = -\frac{g_s}{\tan(2\theta_A)}$, $g_A = \frac{g_s}{\sin(2\theta_A)}$ for the third generation of quarks. The parameters in this model are θ_A and m_A. We vary the value of the coupling in the range $\theta_A \in [0, \frac{\pi}{4}]$, which corresponds to varying the axial and vector couplings from a large value at small θ_A to $g_V = 0$, $g_A = g_s$ for $\theta_A = \frac{\pi}{4}$. A mass range of $m_A \in [1, 3]$ TeV is scanned.

The decay width of the axigluon and the density matrices for top pair production mediated by an axigluon are given in Sec. I of Appendix B. For an s-channel resonance, the terms in the $t\bar{t}$ pair production amplitude which are proportional to the linear power of $\cos\theta$ (where θ is the top-quark polar angle) contribute towards the AFB. The helicity-dependent analysis of the top-quark decay distributions can give additional information about the BSM couplings. We will show in this study that this information can be accessed at the experiments from correlations among top polarization, top-quark and decay-particle asymmetries.

We first discuss constraints coming from $t\bar{t}$-production cross-section measurements, and top-quark-level forward-backward and charge asymmetries measured at the Tevatron and the LHC (as appropriate).

A. Constraints on the axigluon model

We calculate the differential cross section of the process $(pp)p\bar{p} \to t\bar{t} \to l\nu b\bar{t}$ at the Tevatron with $\sqrt{s} = 1.96$ TeV and at the LHC with $\sqrt{s} = 7$ TeV and $\sqrt{s} = 13$ TeV for the SM+BSM with CTEQ6l [59] parton distribution functions with the factorization scale fixed at $Q = 2m_t = 345$ GeV; the top-quark mass is taken to be $m_t = 172.5$ TeV, and $\alpha_s(m_t) = 0.108$.

The cross sections calculated for the Tevatron and LHC, along with the AC and AFB of the $t\bar{t}$ at those experiments in the axigluon model, are shown in Fig. 1. We constrain the model parameter space by limiting the predicted observables $\sigma_{p\bar{p}\to t\bar{t}}$, $\sigma_{pp\to t\bar{t}}$, A_{FB} and A_C to within 2σ of the experimental values. As the values of θ_A and m_A grow larger, the couplings reduce, the mass of the mediating particle rises, and the BSM contributions to the observables reduce. At large values of θ_A, the figures correspond to an axigluon model with only an axial coupling with the top quark and no resulting top polarization. For a lower mass range, constraints from the LHC allow only larger θ_A and hence smaller coupling values; at the same time, interference with SM gives a constraint at the Tevatron which allows some region in the large coupling range as well. A_C gives a complimentary constraint and rules out large values of θ_A (couplings close to g_s) for a smaller mass of the axigluon. The result is that for the low masses of the axigluon, a range of couplings corresponding to $\theta_A \sim (25°–35°)$ and masses $m_A \sim (1300–1900)$ GeV are allowed. Masses above these values are allowed for almost all parameter

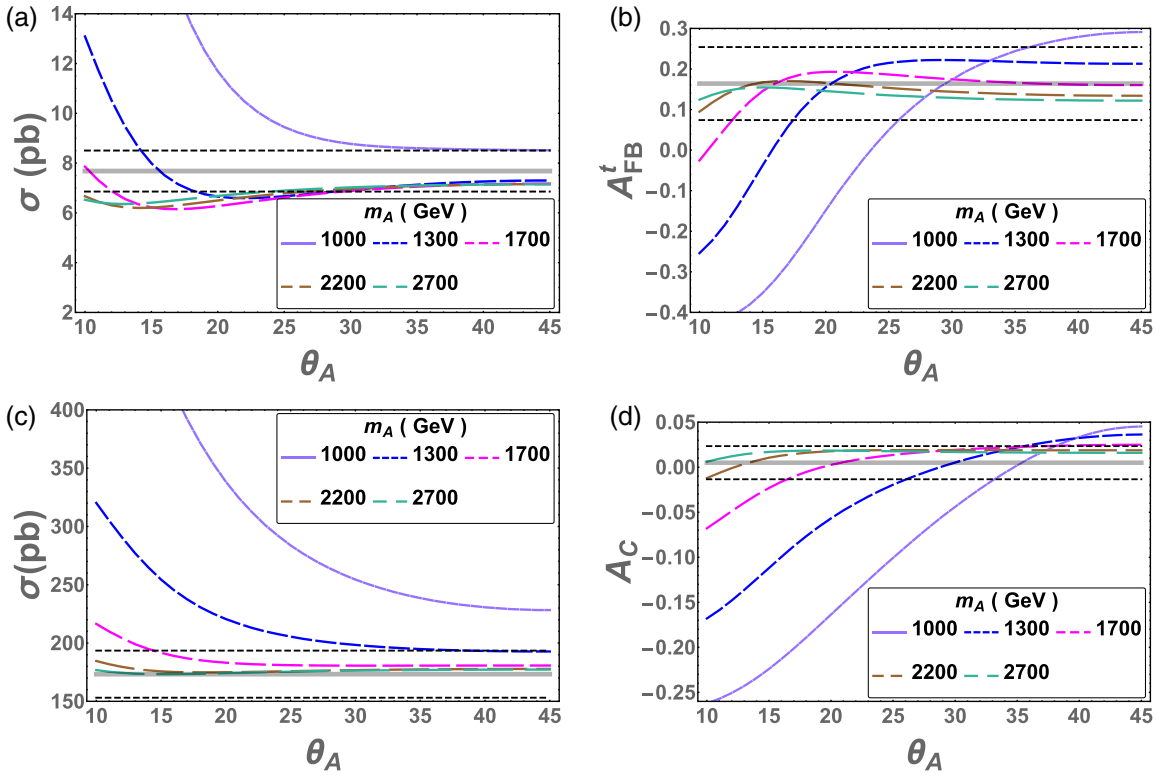

FIG. 1 (color online). The above figure shows the observables: top quark cross section, AFB and AC calculated for the Tevatron and the LHC as functions of θ_A and mass of the axigluon. The experimentally measured values are marked in grey, with the respective 2σ errors shown by dotted black lines. As the lines go from solid to dashed with larger gaps, the mass of the axigluon rises from 1 TeV to 2.7 TeV. The sub-figures represent, (a) cross section at the Tevatron with $\sqrt{s} = 1.96$ TeV; (b) AFB at the Tevatron with $\sqrt{s} = 1.96$ TeV; (c) cross section at the LHC with $\sqrt{s} = 7$ TeV; (d) AC at the LHC with $\sqrt{s} = 7$ TeV.

space, with the only constraints coming from the Tevatron cross section.

CMS results constrain the mass of an additional massive spin-1 color octet of particles (e.g. Kaluza-Klein gluons) which couple to gluons and quarks to above 3.5 TeV, which excludes the parameter region favored by the experimental results from the $t\bar{t}$ process mentioned above [60]. The constraints can be evaded if the assumption of equal couplings of axigluons to light quarks and the top quark is relaxed. In this case, the values of coupling g_V, g_A we use can be split into g_V^q, g_A^q and g_V^t, g_A^t, where the couplings with quarks would be constrained strongly from the axigluon direct production bounds. In the limit that the vector and axial couplings are equal or any one of the vector or axial couplings is small, our results can be recast into the modified model by using $g_{v/a}^2 = g_{v/a}^q g_{v/a}^t$. A more generalized version of such an axigluon model has already been discussed in the literature [61] along with constraints on the model from lepton and top-quark asymmetries at the Tevatron and the LHC.

The axigluon model can be constrained from B physics [62] results, however, given the somewhat large hadronic uncertainties in some of the variables along with the possibility of relaxing these constraints in various modified axigluon models and/or by constructing UV completions. For the purpose of this study, we do not take these constraints into account.

IV. u-CHANNEL SCALAR EXCHANGE MODEL

In a second class of BSM models, AFB is explained due to contributions of a t- or u-channel exchange of new particles between the top quark-antiquark pair. The corresponding mediators do not show resonance behavior and are elusive in the bump-hunting type of analyses in $t\bar{t}$ pair production, though they do contribute significantly to the angular distributions. We consider here a scalar particle called a diquark, which, similar to a squark with R-parity violation, transforms as a triplet under $SU(3)_c$ and has a charge of $-\frac{4}{3}$. The corresponding coupling is given by the Lagrangian

$$\mathcal{L} = \overline{t^c} T^a (y_s + y_p \gamma^5) u \phi_a + \text{H.c.}, \tag{5}$$

$$t^c = -i\gamma^2 t^* = -i(\bar{t}\gamma^0\gamma^2)^T. \tag{6}$$

We assume a right-handed coupling of the scalar with the up-type quarks with $y = y_s = y_p$. This ensures that flavor constraints and proton stability bounds are avoided. The

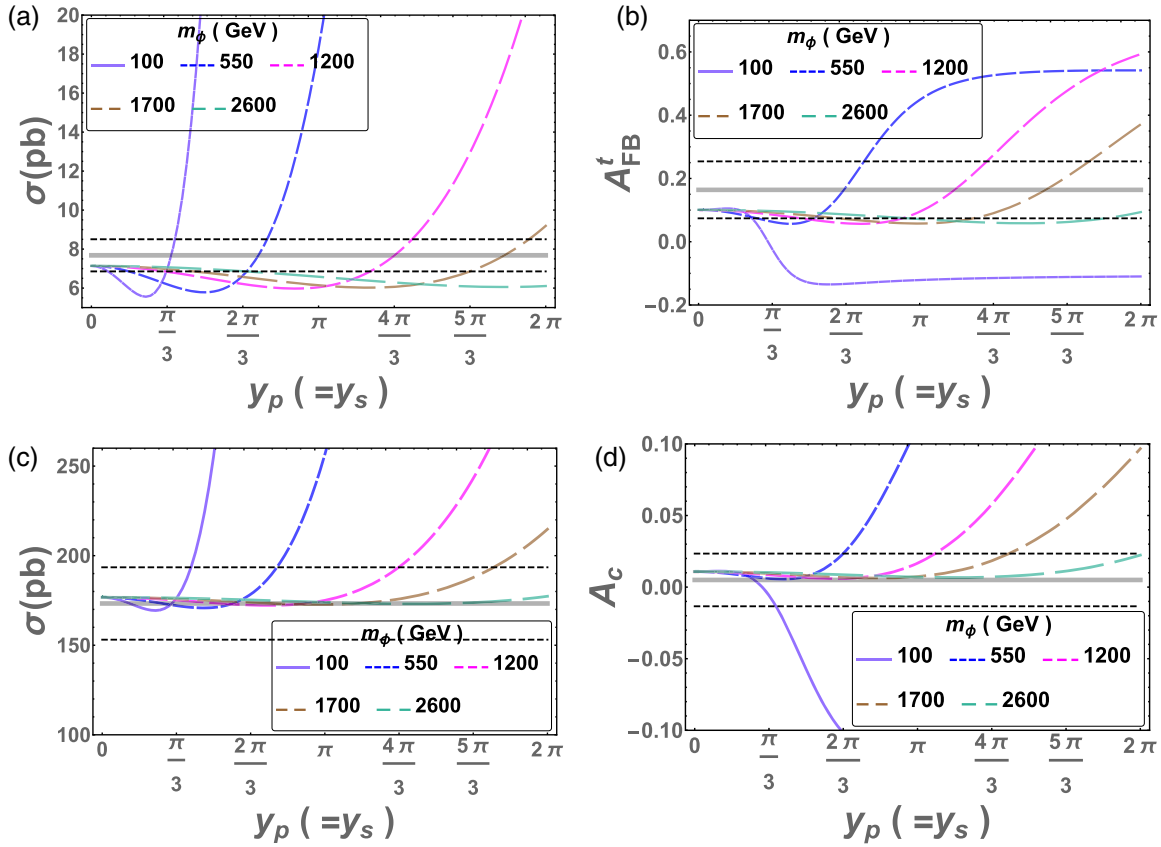

FIG. 2 (color online). The above figure shows the observables: top quark cross section, AFB and AC at the Tevatron and the LHC (7 TeV) as as functions of the Yukawa coupling and for various values of the diquark masses. The experimentally measured values are marked in grey, and the respective 2σ errors are shown by dotted black lines. The line spacing changes from solid to a dashed line with wider spaces as mass values rise from 100–2600 GeV. The sub-figures show respectively, (a) The cross section at the Tevatron $\sqrt{s} = 1.96$ TeV; (b) AFB at the Tevatron $\sqrt{s} = 1.96$ TeV; (c) cross section at the LHC $\sqrt{s} = 7$ TeV; (d) A_C at the LHC $\sqrt{s} = 7$ TeV.

density matrices for top pair production in the diquark model are given in Sec. II of Appendix B. All calculations in this work are performed at tree level. The NLO contributions become important to studying the effects on invariant mass distributions which we have not included here. These calculations are under progress for both axigluon and diquark models.

A. Constraints on the colored scalar model

As in the case of an s-channel resonance in the previous section, the constraints are obtained from the measurements of the top pair production cross section at the Tevatron and the LHC (7 TeV), the AFB and AC. We explore a parameter space of $m_\phi \in [100, 3000]$ GeV and $y \in [0, 2\pi]$, chosen so as to explore all the values of the coupling within the perturbative limit. As the value of the coupling rises, contribution of the BSM to all the observables becomes larger. For lighter diquarks, negative values of AFB and AC are predicted for large values of the coupling, though this mass range is ruled out by independent constraints from diquark pair production [63]. In Fig. 2, we can notice from the top-left panel that, as in the case of the axigluon, the Tevatron cross section provides the constraints in the parameter space of lower masses and couplings. In the next panel, the AFB measured at the Tevatron disallows lighter scalars and also constrains a part of the coupling values for larger masses. The LHC cross section constrains large coupling regions which give a larger contribution, and the cutoff coupling increases as the mass of the scalar becomes heavier. The AC also allows larger coupling parameter space for higher masses of the scalar.

The constraints from pair production of the colored scalar from gluon fusion at the LHC are weak (~300 GeV) as reinterpreted from corresponding constraints on squarks [64]. There are further constraints on lower-mass scalars from atomic parity violation [65]. Constraints from $uu \to tt$ can be avoided by adding flavor symmetries (see for example Ref. [66]).

V. CONSTRAINTS FROM DIJET PRODUCTION AT LHC

The colored scalar and vector BSM models get constrained from searches for direct production of BSM particles and subsequent decay to dijet and four-jet final

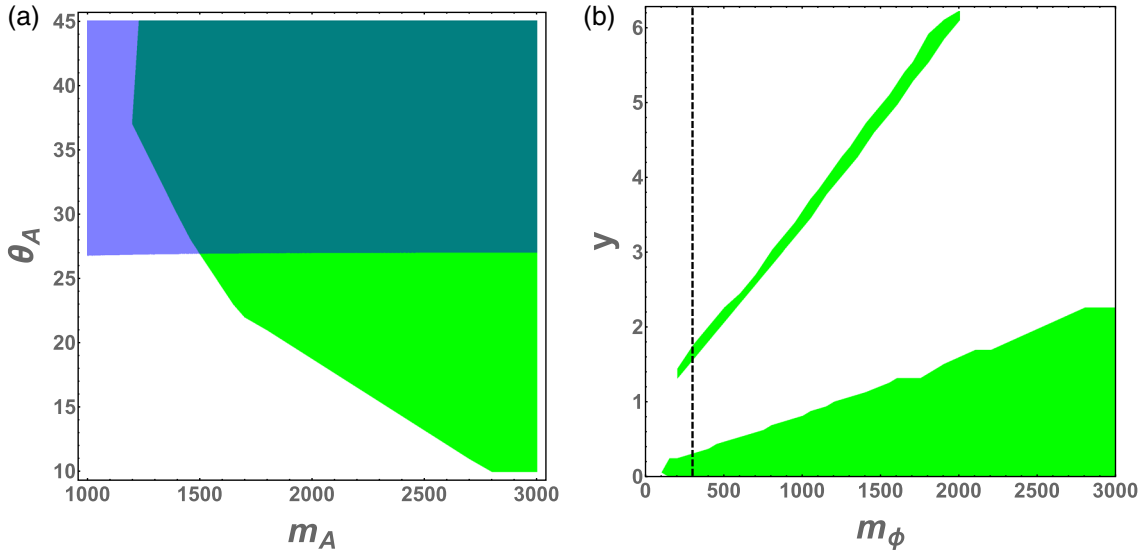

FIG. 3 (color online). In the figures above, allowed parameter space for axigluon and diquark models are depicted as green (lighter) colored regions. (a) Shows constraints on the parameter space of axigluon model where, the blue (darker) shaded area shows the constraints from dijet searches. (b) Shows constraints on diquark model parameter space and the dotted line represents the bound from pair production of BSM particles at LHC.

states ($q\bar{q} \to A \to 2j$, $gg \to \phi\phi^\dagger \to 4j$). Earlier constraints on the axigluon model were obtained from searches of narrow resonances from the dijet spectrum at 8 TeV LHC and were extended to the case of a wider axigluon model with $\frac{\Gamma_A}{m_A} = 0.3$, where the axigluon has only axial-vector couplings [67] (see also Ref. [68] for BSM particle off-shell effects in dijet searches). We reinterpret these constraints to the case of the axigluon model in this study, which has both axial-vector and vector couplings with the quarks, and find the excluded parameter range where $\frac{\Gamma_A}{m_A} < 0.3$. Figure 3(a) shows the parameter space allowed for the axigluon model. The following constraints are put on the model parameters to obtain the allowed values: reinterpreted searches for BSM resonances in dijet production, $t\bar{t}$ cross section and top charge asymmetry measurements at 7 TeV LHC and cross-section top forward-backward asymmetry measurements at the Tevatron as discussed in Sec. III A. The coupling values corresponding to $\theta_A > 27°$ are ruled out for axigluon masses up to ~4 TeV, as these narrow, resonant particles would have been detected in the dijet searches. The allowed values of couplings correspond to $\theta_A \sim 10°$–$27°$ for the mass range between 1.5 TeV and 3 TeV. Note that the constraints from dijet searches may be relaxed if the magnitude of the coupling of axigluons is different for the third generation of quarks as compared to the first and the second generations.

The diquark mass is bound from below to $m_\phi >$ ~300 GeV from pair production of diquarks via gluon fusion at the LHC [64]. The direct production bounds along with the constraints obtained from top-quark pair production cross section and top charge forward-backward asymmetry measurements at the LHC and Tevatron (see Sec. IV) are shown in Fig. 3(b). A narrow strip of parameter space is allowed when couplings are large due to destructive interference effects. Besides this region, the rest of the allowed diquark parameter space follows the expected behavior of small coupling values < 0.2 for lower masses, and for a diquark of mass 3 TeV, y_s as large as 2 is allowed.

VI. POLARIZATION OF THE TOP-QUARK AND DECAY-LEPTON DISTRIBUTIONS

The decay kinematics of leptons embeds the information regarding top-quark production dynamics, kinematics and polarization [20]. Different lepton observables embed these effects in different ways and so provide a number of probes which are all correlated with the top-quark kinematics and polarization. For a detailed analysis of top-quark decay, see Refs. [31,32]. In this section, we discuss distributions of the lepton polar angle, azimuthal angle and energy in SM decay of top-quark and construct asymmetries based on these distributions to probe top-quark BSM interactions.

A proper treatment of the decay distributions of the top quark requires the spin-density matrix formulation, which preserves correlations between the spin states in the production and in the decay.

The spin-density matrix for t in the production of a $t\bar{t}$ pair with the spin of $\bar{t}$ summed over can be expressed as

$$\rho_{t\bar{t}\,\text{production}}(\lambda_t, \lambda_t') = \sum_{\lambda_{\bar{t}}} \mathcal{M}_{\text{production}}(\lambda_t, \lambda_{\bar{t}}) \mathcal{M}^\star_{\text{production}}(\lambda_t', \lambda_{\bar{t}}). \tag{7}$$

The density matrix gets SM contributions $\rho^{gg}_{\text{SM}}(\lambda_t, \lambda_t')$ and $\rho^{q\bar{q}}_{\text{SM}}(\lambda_t, \lambda_t')$ from gluon-gluon and quark-antiquark initial states, respectively, a contribution $\rho_{bSM}(\lambda_t, \lambda_t')$ from the

BSM model, and a contribution $\rho_{\text{interference}}(\lambda_t, \lambda_t')$ from the interference between the SM amplitude and the BSM amplitude:

$$\rho(\lambda_t, \lambda_t') = \rho_{\text{SM}}^{gg}(\lambda_t, \lambda_t') + \rho_{\text{SM}}^{q\bar{q}}(\lambda_t, \lambda_t') + \rho_{bSM}(\lambda_t, \lambda_t') + \rho_{\text{Interference}}(\lambda_t, \lambda_t'). \quad (8)$$

The spin-density matrix for the decay of the top quark is given by

$$\Gamma_{\text{top decay}}(\lambda_t, \lambda_t') = \mathcal{M}_{\text{decay}}(\lambda_t)\mathcal{M}^{\star}_{\text{decay}}(\lambda_t'), \quad (9)$$

with the spins of the decay products summed over.

The squared amplitude for the combined process of production and decay is given by

$$\overline{|\mathcal{M}|^2} = \frac{\pi\delta(p_t^2 - m_t^2)}{\Gamma_t m_t}\sum_{\lambda_t, \lambda_t'}\rho(\lambda_t, \lambda_t')\Gamma(\lambda_t, \lambda_t'). \quad (10)$$

This expression assumes a narrow-width approximation for the top quark. Top decay is assumed to progress through SM processes. In the rest frame of the top quark, the differential decay distribution of the top quark is given by

$$\frac{d\Gamma_t}{\Gamma d\cos(\theta)} = \frac{1 + A_p k_f \cos\theta}{2}, \quad (11)$$

where θ is the angle between top-quark spin direction and the momentum of the decay product f. For $N(\lambda_t)$ number of top quarks with helicity λ_t, polarization A_p is defined as

$$A_P = \frac{N(\lambda_t = +) - N(\lambda_t = -)}{N(\lambda_t = +) + N(\lambda_t = -)}, \quad (12)$$

and the coefficient k_f is called the top-spin analyzing power of the decay particle f. For the case of leptons as the final state particles, the factor $k_f = 1$ at tree level in the SM. When the top quark is boosted in the direction of its spin quantization axis, Eq. (11) gets modified to

$$\frac{\mathrm{d}\Gamma^{\text{Boosted}}}{\Gamma \mathrm{d}\cos(\theta_{tl})} = \frac{(1-\beta^2)(1 + \lambda_t\cos\theta_{tl} - \beta(\cos\theta_{tl} + \lambda_t))}{2(1 - \beta\cos\theta_{tl})^3}, \quad (13)$$

where θ_{tl} is defined as the angle between the lepton and top-quark momenta in the boosted frame. Lepton kinematic distributions for the tree-level SM differential cross section for the process $p\bar{p} \to t\bar{t} \to l + \text{jets}$ with $\sqrt{s} = 1.96$ TeV are presented in Fig. 4. The energy and azimuthal lepton distributions are uncorrelated with the polarization in the rest frame of the top quark, though they correlate with the polarization in the boosted frame. Higher-order corrections to the production and decay processes have been calculated for the SM, and the distributions are found to be qualitatively unchanged [69,70]. Due to this, we expect the effect of higher-order corrections to the asymmetries constructed from decay-lepton distributions to be relatively small, as the corrections partially cancel out within the difference and ratio taken to derive the asymmetry.

A lepton polar-angle asymmetry with respect to the top-quark direction can be defined by

$$A_{\text{FB}}^{tl} = \frac{\sigma(\cos(\theta_{tl}) > 0) - \sigma(\cos(\theta_{tl}) < 0)}{\sigma(\cos(\theta_{tl}) > 0) + \sigma(\cos(\theta_{tl}) < 0)}. \quad (14)$$

A_{FB}^{tl} has been measured at both LHC and Tevatron in the lab and in the $t\bar{t}$ center-of-momentum frame, albeit with large statistical errors and different results from CDF and D0 [49]. Integrating Eq. (11), the top rest-frame lepton asymmetry can be related to the polarization of the top quark,

$$A_P = \frac{1}{2}A_{\text{FB}}^{tl,t-\text{rest}}. \quad (15)$$

In QCD, $A_{\text{FB}}^{tl,\text{rest}} = A_p = 0$, though in the boosted frame, the lepton polar asymmetry with respect to the top quark is large even in a tree-level SM calculation.

In the lab frame where the top quarks and leptons are boosted and the cross section convoluted with the PDF, the correlations between various angles and energies become more complicated. The lepton polar angle with respect to the proton beam is a convenient observable which does not require top-quark rest-frame or momenta reconstruction. The lepton polar asymmetry A_{FB}^{l} in the lab frame is also 0 at tree level in SM QCD. A_{FB}^{l} is identically 0 at the LHC due to the symmetric nature of the initial state. This asymmetry, according to our analysis, correlates the best with the off-diagonal elements of the top-quark density matrix for the $l + \text{jets}$ process considered (see Sec. VIII) for both axigluon and diquark models. An analytic study of the lepton polar angle and its correlation with top AFB and polarization has also been made by Berger *et al.* [71]. They relate the lepton and the top-quark level polar asymmetries and subsequently use this relation to distinguish between a sequential axigluon and a W'-type model [72].

In the top-quark rest frame, other lepton kinematic variables—azimuthal angle and its energy—have no dependence on the helicity of the top quark, and hence the integrated asymmetries are uncorrelated with the polarization. It has been noted in the literature that the lepton azimuthal distributions correlate with the polarization of the top quark in a boosted frame [32,73–75]. Sums and differences of the azimuthal decay angle in the top pair production process have also been used in the literature to study the polarization and spin correlations of the top quark in detail [76]. For a detailed analysis of analytic relation between polarization of a heavy particle and decay particle azimuthal asymmetry, see Ref. [77]. We reproduce the azimuthal distribution in the lab frame for the SM $t\bar{t}$ pair production process at the Tevatron in Fig. 4(c). The azimuthal distribution can be measured at both Tevatron and the LHC and requires only

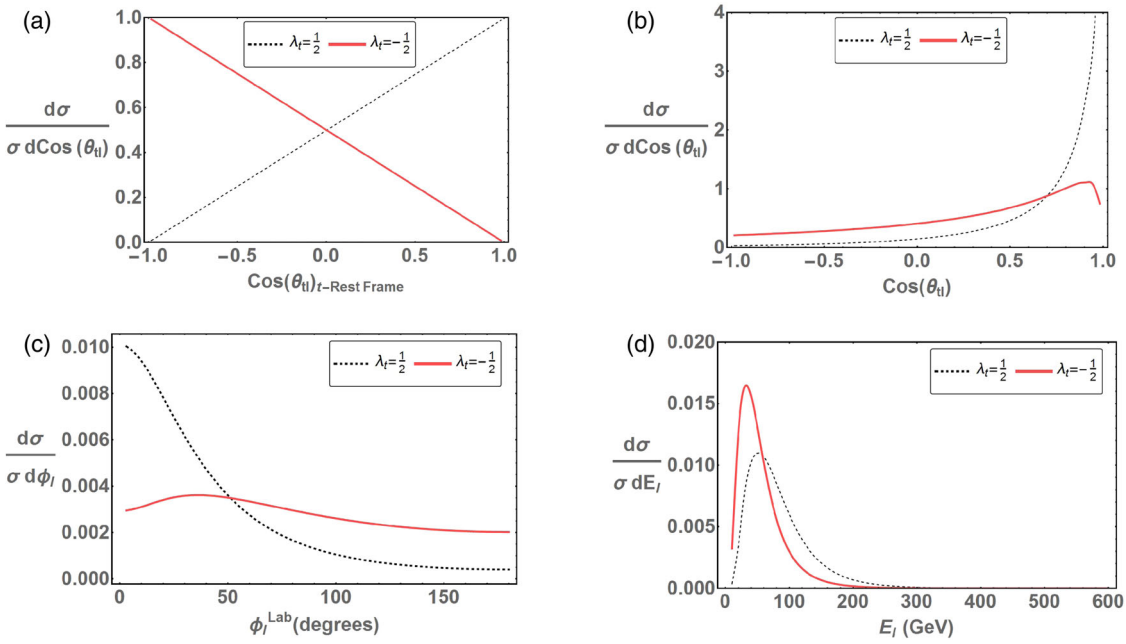

FIG. 4 (color online). The tree-level lepton polar and azimuthal distributions for $p\bar{p} \to t\bar{t} \to l + \text{jets}$ with $\sqrt{s} = 1.96$ TeV. In the above plots, the average boost of the $t\bar{t}$ pairs is 0.34. (a) Lepton polar angle distribution in top quark rest frame; (b) Lepton polar angle distribution in the lab frame; (c) Lepton Azimuthal angle distribution in the lab frame; (d) Lepton energy distribution in the lab frame.

partial reconstruction of the top-quark rest frame. The azimuthal angle is defined by assuming that the top quark lies in the x-z plane with the proton (beam) direction as the z-axis. From this distribution, an azimuthal asymmetry about a point ϕ_0 can be defined as

$$A_\phi^l = \frac{\sigma(\pi > \phi_l > \phi_0) - \sigma(\phi_l < \phi_0)}{\sigma(\pi > \phi_l > \phi_0) + \sigma(\phi_l < \phi_0)}. \tag{16}$$

A natural choice for the value of ϕ_0 would be the point of intersection of the distributions corresponding to left- and right-helicity top quarks. For SM, this point is about $\phi = 50°$ for both Tevatron and the LHC. The SM point would correspond to 0 polarization and would maximize correlation with BSM contribution. We assume a value of ϕ_0 a bit lower at 40°. Since the positive-helicity top quarks have a larger differential cross section in this region, this choice enhances correlations of the lepton level asymmetry for larger positive (or smaller negative) values of polarization. The standard-model tree-level results for this asymmetry at the Tevatron and the LHC are given in Table IV. In the lab frame, due to the boost and rotation from the direction of the top quark, A_ϕ is sensitive to both the polarization and the parity-breaking or t-channel structure of the top-quark coupling. Another observable which can be constructed from the decay-lepton kinematics is the lepton energy asymmetry about a chosen energy E_0:

$$A_{E_l}^l = \frac{\sigma(E_l > E_0) - \sigma(E_l < E_0)}{\sigma(E_l > E_0) + \sigma(E_l < E_0)}. \tag{17}$$

No reconstruction of the top-quark rest frame is needed to measure E_l. Just like the azimuthal case, this asymmetry can be measured at both the LHC and the Tevatron. The lepton energy distribution is sensitive to the polarization of the top quark [32], as shown in Fig. 4(d). Similar asymmetries based on the energy of decay particles or the ratios of these energies have been used in the literature to study BSM physics [74,78–80]. We define the lepton energy asymmetry about

TABLE IV. Scale dependence of SM values of various asymmetries at tree level.

(a) Tevatron $\sqrt{s} = 1.96$ TeV		
Asymmetry	$Q = m_t$	$Q = 2m_t$
A_{FB}^{tl}	0.645	0.642
A_ϕ^l	−0.113	−0.116
$A_{E_l}^l$	0.381	0.397
(b) LHC $\sqrt{s} = 7$ TeV		
Asymmetry	$Q = m_t$	$Q = 2m_t$
A_{FB}^{tl}	0.748	0.748
A_ϕ^l	−0.075	−0.077
$A_{E_l}^l$	0.138	0.146
(c) LHC $\sqrt{s} = 13$ TeV		
Asymmetry	$Q = m_t$	$Q = 2m_t$
A_{FB}^{tl}	0.789	0.788
A_ϕ^l	−0.041	−0.044
$A_{E_l}^l$	0.036	0.038

a value of $E_0 = 80$ GeV, to act as a better discriminator between BSM and SM. Ideally, the point of intersection of the positive and the negative top polarization curves should form the best correlation with the top polarization, though this point varies with the energy and the invariant mass of the initial state. Standard-model values of asymmetries mentioned in this section are given in Table IV. It would be interesting to use SM distributions at NLO to decide the reference points E_0, ϕ_0, but since in the end we construct asymmetries, we expect that the qualitative behavior of our results would not change.

In the recent past, polarization measurements have been made by collaborations at both the Tevatron and the LHC. The polarization at the Tevatron points towards a small positive value, and that at the LHC to small negative values. This is consistent with the small-coupling and large-mass regimes of both the models studied here.

In the next section, we use correlations among top charge and forward-backward asymmetries, decay lepton angular and energy asymmetries, and polarization to uncover specific properties of BSM particles which can be inferred from the Tevatron and the LHC data.

VII. CORRELATIONS

The parameter space of $m_A \in [1000, 3000]$ GeV and $\theta_A \in [10, 45]$ is explored for the axigluon model, and that of $m_\phi \in [100, 3000]$ GeV and $y_s \in [0, 2\pi]$ for the colored scalar. The figures in Sec. VII B show parameter space allowed by the constraints mentioned in Secs. III and IV.

A. Correlations between charge and forward-backward asymmetries

The correlation between the AC at 7 TeV LHC and the AFB at the Tevatron have been used in the literature to constrain various BSM models (see, for example, Ref. [14]). These constraints are model dependent, and the asymmetries are not in general tightly correlated [81]. We show similar correlations in Fig. 5, where we plot A_C vs $A_{\rm FB}$, using the relation

$$A_{C/\rm FB} = A_{C/\rm FB}^{\rm SM\_NLO} + A_{C/\rm FB}^{bSM}. \tag{18}$$

This relation is valid as long as the BSM physics corrects the SM cross section of the $t\bar{t}$ pair production process by a small amount.

The pure axial axigluon which leads to an unpolarized top quark is disfavored, as it does not have a parameter space where it can explain both $A_{\rm FB}$ and A_C experimental values. In the diquark model, the coupling to right-handed quarks is sampled from 0 to 2π, where large mass or small couplings lead to a better agreement with SM NLO values of asymmetries.

B. Correlations among lepton and top asymmetries

In this section, we study the correlations among top polarization, top asymmetries and decay-lepton asymmetries. We show that combined, they form sensitive discriminators between models with different dynamics. The top-quark and decay-lepton asymmetries are calculated at various points in the parameter space allowed by the experimental constraints discussed in Secs. III and IV. The expected polarization of the top quark, for corresponding points in the parameter space, is represented in color-contrast form inside the graphs, and clear trends for the polarization can be observed. In all the following figures, top-quark asymmetries represented on the x-axis are calculated as shown in Eq. (18), and the lepton asymmetries shown on the y-axis are calculated, including SM + BSM contributions at tree level.

1. Asymmetry correlations for the Tevatron

The correlations of the lepton-level asymmetries with the top AFB at the Tevatron are shown in Figs. 6(a), 6(b), 7(a)

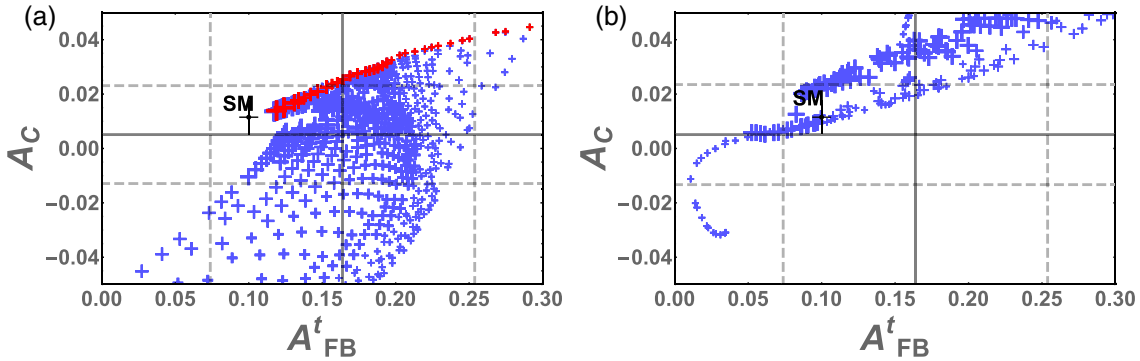

FIG. 5 (color online). Correlation between top-quark asymmetries AFB vs AC at the Tevatron and the LHC ($\sqrt{s} = 7$ TeV). The grey solid and dashed lines represent the observed values of the respective asymmetries and their 2σ errors. The sub-figures respectively represent, (a) The axigluon model, with the red markers representing only axial interactions ($g_V = 0$, $g_A^t = g_s$) (unpolarized top quark in final sate). The size of the plus marks represent a mass range from 1000–3000 GeV; (b) The diquark model. The size of the plus marks represent a mass range from 100–3000 GeV.

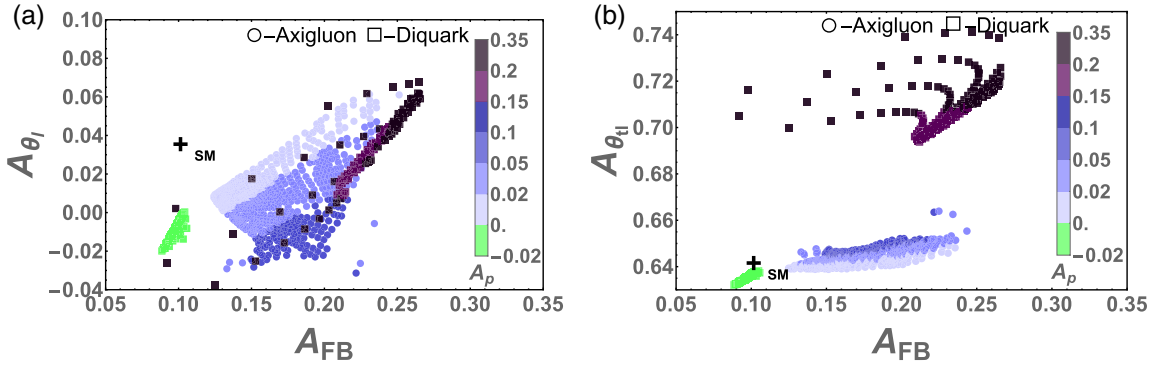

FIG. 6 (color online). Correlations between top AFB and lab frame θ_l, θ_{tl} asymmetries at the Tevatron $\sqrt{s} = 1.96$ TeV. (a) Lepton polar asymmetry (w.r.t beam direction) ; (b) Lepton polar asymmetry (w.r.t top quark direction).

and 7(b). For the case of the axigluon, as its mass is increased, the polarization rises until $m_A \sim 1650$ GeV and then drops again for even larger masses. The diquark model predicts negative polarization for a significant portion of parameter space, turning positive only for large couplings. The large-mass region for the diquark also favors large (negative) values of azimuthal asymmetry, smaller lepton polar asymmetry and larger lepton energy asymmetry. Lepton polar asymmetry correlation with top AFB shows large overlap between the two models. The observed value for the lab-frame lepton polar asymmetry in Tables II and III points towards a positive polarization between $A_{\theta_l} = 0.2$ and 1.1. In this region [see Fig. 6(a)], a large positive value for polarization is favored for the diquark model and a large contribution to top AFB. The axigluon model is compatible with both the observed value of A_{θ_l} and a small contribution towards longitudinal polarization for a significant part of its parameter space. Figure 6(b) shows the asymmetry in the lepton polar angle with respect to the top direction, $A_{\theta_{tl}}$, which is equal to twice the top polarization [Eq. (15)] when calculated in the top-quark rest frame. It receives a contribution from BSM physics via the boost of the parent top quark. In the lab frame, large deviations of $A_{\theta_{tl}}$ from the SM value correlate with a large contribution to the top-quark polarization from the BSM. The values of the asymmetries grow closer to the corresponding SM values with an increase in mass and a reduction in the BSM coupling strength. The azimuthal asymmetry and lepton polar asymmetry with respect to the top-momentum direction ($A_{\theta_{tl}}$) and lepton energy asymmetry in Figs. 6(b), 7(a) and 7(b) discriminate well between the s-channel and u-channel exchange models, though the parameter spaces within the model are clumped together. When combined with polarization, all correlations enhance their discriminating power, especially to distinguish between s-channel and u-channel models, as they predict opposite signs of polarization for a large portion of parameter space.

2. Asymmetry correlations for the LHC

The lepton-level asymmetry correlations with $t\bar{t}$ charge asymmetry are shown in Figs. 8(a)–8(c) for the LHC 7 TeV run and in Figs. 9(a)–9(c) for the LHC 13 TeV run. The plots are made for the region of the model parameter space constrained in Secs. III and IV. For the $\sqrt{s} = 7$ TeV calculation, we use $m_t = 172.5$ GeV and factorization scale $Q = 2m_t$ and $\alpha_s = 0.108$ to remain consistent with

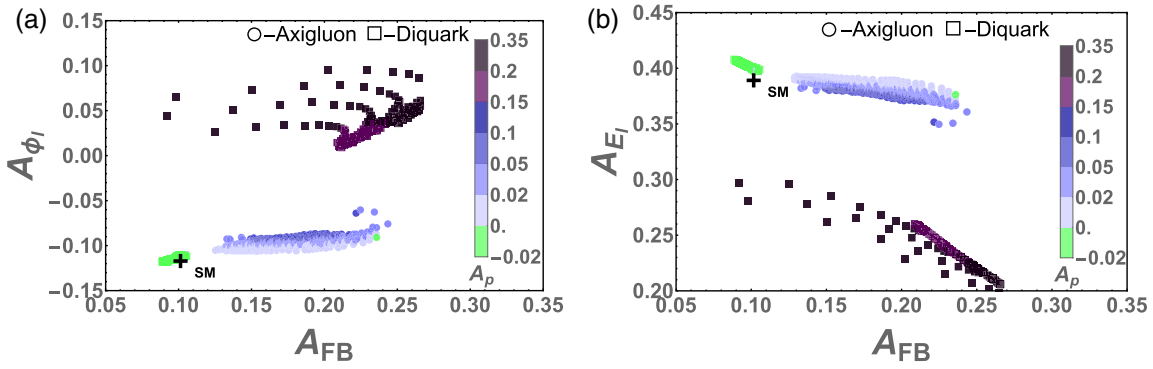

FIG. 7 (color online). Correlations between top AFB and the lepton energy and azimuthal asymmetries at the Tevatron $\sqrt{s} = 1.96$ TeV. (a) Lepton azimuthal asymmetry about $\phi_0 = 40°$; (b) Lepton energy asymmetry about the energy $E_0 = 80$ GeV.

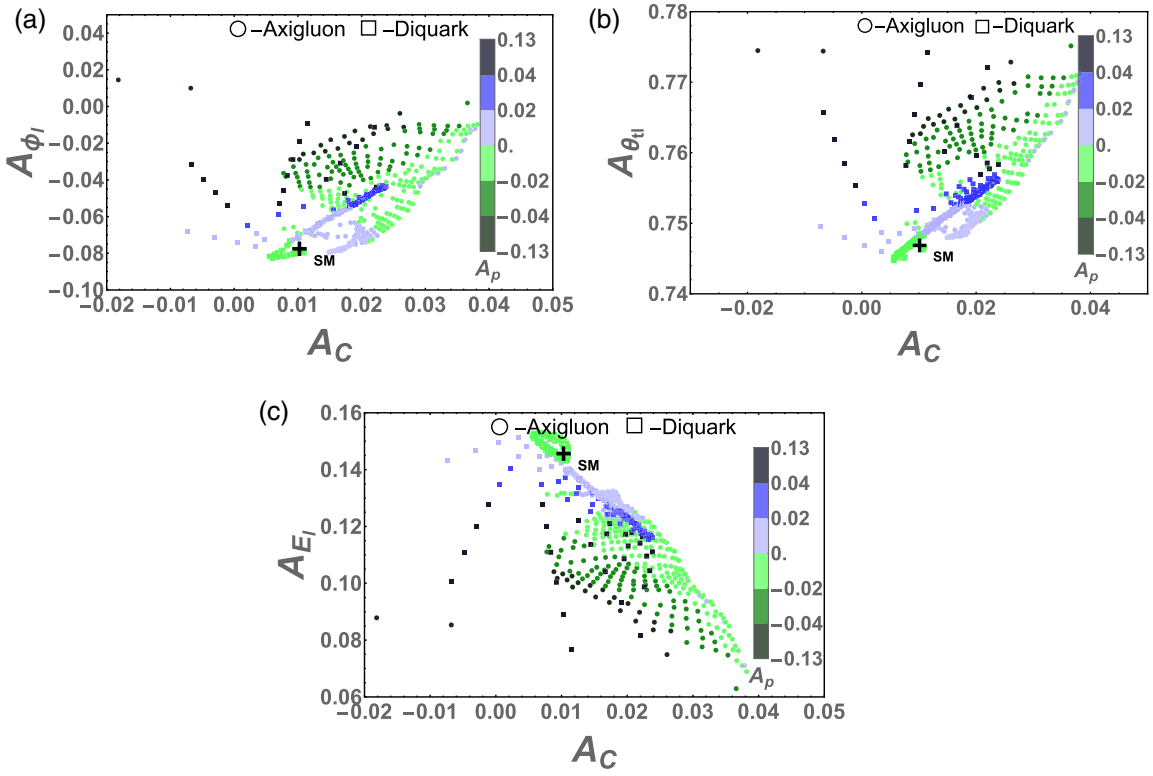

FIG. 8 (color online). Correlations between top AC and lepton kinematic asymmetries at the LHC $\sqrt{s} = 7$ TeV. The sub-figures represent correlations with the following lepton asymmetries, (a) Lepton azimuthal asymmetry about $\phi_0 = 40$; (b) Lepton polar asymmetry(w.r.t top quark direction); (c) Lepton energy asymmetry about $E_0 = 80$ GeV.

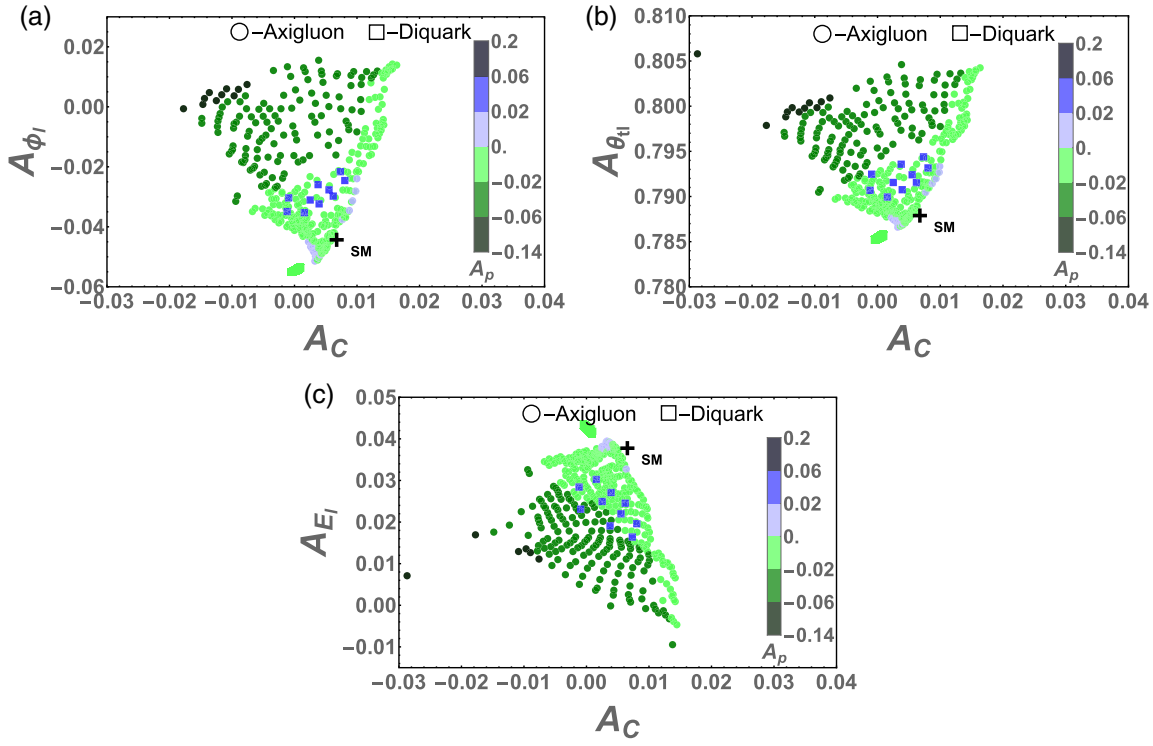

FIG. 9 (color online). Correlations between top AC and lepton kinematic asymmetries at the LHC $\sqrt{s} = 13$ TeV. The sub-figures represent correlations with the following lepton asymmetries, (a) Lepton azimuthal asymmetry about $\phi_0 = 40$; (b) Lepton polar asymmetry(w.r.t top quark direction); (c) Lepton energy asymmetry about$E_0 = 80$ GeV.

the ATLAS and CMS reconstruction of A_C. For $\sqrt{s} = 13$ TeV, the mass of the top quark is chosen at the updated central value $m_t = 173.2$ GeV and $Q = 2m_t$ with $\alpha_s = 0.108$ and CTEQ6l PDF.

A large portion of the parameter space predicts a negative polarization at 7 TeV LHC for the axigluon model. The diquark model predicts a small negative polarization for small couplings with quarks. When heavier diquark models are considered, larger couplings are allowed, leading to a large positive contribution to the polarization. Observed values of polarization from CMS and ATLAS are compatible with $-0.03 < A_p < 0.07$, which covers a large region of parameter space for both axigluon and diquark models. As in the case of the Tevatron, polarization is an important discriminant between models for the LHC as well, especially when combined with decay-lepton asymmetries. It is able to distinguish overlapping parameter space regions between the two models. This is more true when the couplings are small and the BSM effects are more difficult to detect, as the s-channel and u-channel exchanges predict small polarization, but with opposite signs in this region. The energy asymmetry becomes smaller for the LHC at 13 TeV due to the effect of the overall boost. The values of azimuthal and polar asymmetries do not change significantly for higher energy and so remain good observables for the study of top-quark dynamics.

VIII. ASYMMETRY CORRELATIONS AND TOP TRANSVERSE POLARIZATION

As remarked earlier, keeping full spin correlations between the production and decay of the top quark in a coherent manner requires the spin-density matrix formalism. In this formalism, the top polarization, which played a significant role in the above analysis, corresponds to the difference in the diagonal elements of the density matrix, as seen from Eq. (12). The off-diagonal elements of the density matrix can also be significant in practice, and they would contribute to the transverse polarization of the top quark, corresponding to a spin quantization axis transverse to the momentum. In SM, these terms arise at loop level and have been studied in the literature along with transverse polarization, and observables have been suggested to measure their contribution [82]. We examine in this section what role these off-diagonal matrix elements and transverse top polarization play in the two models considered in this study.

Following the formalism developed in Ref. [32], the spin-density matrix integrated over a suitable final-state phase space can be written as $\sigma(\lambda, \lambda') = \sigma_{\rm tot}\mathcal{P}_t(\lambda, \lambda')$, where $\sigma_{\rm tot}$ represents the unpolarized cross section. The matrix $\mathcal{P}_t(\lambda, \lambda')$ can be written as

$$\mathcal{P}_t(\lambda, \lambda') = \begin{pmatrix} 1+\eta_3 & \eta_1 - i\eta_2 \\ \eta_1 + i\eta_2 & 1-\eta_3 \end{pmatrix}. \tag{19}$$

Here η_3 is the longitudinal polarization, and η_1 and η_2 are polarizations along two transverse directions. The expressions for the η_i in terms of the top-quark density matrix $\sigma(\lambda_t, \lambda_t')$ can be written as

$$\eta_3 = \frac{(\sigma(++) - \sigma(--))}{\sigma_{\rm tot}}, \tag{20}$$

$$\eta_1 = \frac{(\sigma(+-) + \sigma(-+))}{\sigma_{\rm tot}}, \tag{21}$$

$$i\eta_2 = \frac{(\sigma(+-) - \sigma(-+))}{\sigma_{\rm tot}}. \tag{22}$$

Splitting the top density matrix as shown in Eq. (10) under the narrow-width approximation, the helicity-dependent decay density matrix in the rest frame of the top quark separates into a simple function of the decay angle:

$$d\Gamma(\lambda, \lambda') = c \times A(\lambda, \lambda') d\Omega_l, \tag{23}$$

where

$$A = \begin{array}{c|cc} \lambda\downarrow, \lambda' \rightarrow & + & - \\ \hline + & 1+\cos(\theta_l) & \sin(\theta_l)e^{i\phi_l} \\ - & \sin(\theta_l)e^{-i\phi_l} & 1-\cos(\theta_l). \end{array} \tag{24}$$

Ω_l is the solid angle in which the lepton is emitted, and c is the integrated contribution of the rest of the decay kinematic variables. The resulting lepton angular distribution in the lab frame is

$$\frac{d\sigma}{d\cos(\theta_l)d\phi_l} = c\sigma_{\rm tot}(1 + \eta_3\cos(\theta_l) + \eta_1\sin(\theta_l)\cos(\phi_l) + \eta_2\sin(\theta_l)\sin(\phi_l)). \tag{25}$$

The off-diagonal elements in the top-quark production density matrix do not contribute to the total cross section due to an overall factor of $\sin(\theta_l)$ which integrates to 0. They do contribute instead to the kinematic distributions of the decay particle, although this effect is quite small for most observables.

In this study, we find that the lepton polar angle asymmetry defined in the lab frame is sensitive to the off-diagonal terms in the top-quark density matrix [Eq. (7)]. The transverse polarization originating from these off-diagonal terms contains further information about the dynamics of top-quark interaction. This relation has been pointed out before in the context of a wide color octet BSM particle [83,84].

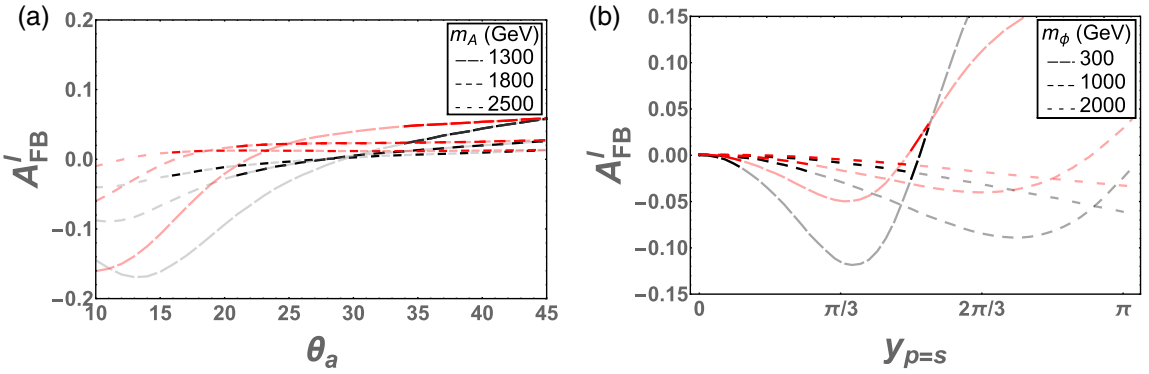

FIG. 10 (color online). Contribution to lepton asymmetry from the off-diagonal terms of the top density matrix calculated in the lab frame for the Tevatron $\sqrt{s} = 1.96$ TeV for the axigluon and diquark models. The red lines represent the asymmetry for a diagonal density matrix, and the black line represents the distribution for the case of a total density matrix. The darker lines represent allowed regions of parameter space. (a) axigluon; (b) diquark.

In Fig. 10, we study the contribution of off-diagonal terms to the lepton distributions and present the distributions for a few sample masses of BSM particles.

It can be seen that the contribution of the off-diagonal density matrix elements can be significant, and it is particularly important for the diquark model. These can in turn lead to significant transverse polarization of the top for an appropriate range of parameters which could be measured experimentally.

IX. CONCLUSIONS

The forward-backward asymmetry of the top quark in the top pair production process at the Tevatron collider was, for a long time, anomalously large and a persistent effect observed independently by both D0 and CDF detectors. It has been demonstrated only relatively recently that NNLO contributions give rise to an $A_{\rm FB}^t$ of the right order of magnitude and seem to be in agreement with the values measured experimentally. Previously, many BSM models had been proposed with parity-breaking interactions to explain the observed $A_{\rm FB}^t$. Many of these models predicted a charge asymmetry at the LHC. Since LHC has a gluon-dominated initial state as opposed to the Tevatron, where $q\bar{q}$ was the primary initial state, the asymmetries predicted for LHC coming from the BSM couplings to the quarks get diluted. The data give values for A_C consistent with the SM, and so far there has been no evidence for the new particles predicted in the different BSM models. Under these circumstances, there is a need to construct measures which can distinguish between different sources of the $A_{\rm FB}^t$: either SM or BSM.

One such measure is provided by polarization of the top quark which has a nonzero value in the presence of a parity-breaking interaction. Within SM, top polarization is close to 0. Observables that correlate with top polarization can be used to distinguish between various SM and BSM contributions. In continuation to a previous work where correlations between polarization and forward-backward asymmetry were used to constrain BSM [14], we have introduced the correlations between lepton polar, azimuthal and energy asymmetries and top charge asymmetry and showed how they can be used together with top longitudinal polarization to distinguish between SM and BSM.

In Ref. [85], the authors have constructed dilepton central charge and azimuthal asymmetries and studied them along with top-quark polarization, forward-backward asymmetry and $t\bar{t}$ spin correlations for benchmark models of G' and W'. Subsequently, in Ref. [71], the authors have shown that the lepton polar asymmetry and top forward-backward asymmetry and lepton charge asymmetry vs top charge asymmetry correlations can be useful in the study of W' and G' models. Our work adds multiple new observables to the analysis of new physics in $t\bar{t}$ pair production, which include single-lepton azimuthal angle, energy and polar angle (with respect to the top quark) in the lab frame, which show signatures from parity breaking in top interactions and help isolate and constrain the interactions of BSM particles.

We demonstrate the efficacy of the correlations between forward-backward asymmetry and the lepton asymmetries at the Tevatron and between charge asymmetry and lepton angluar energy asymmetries at the LHC by utilizing a representative s-channel model axigluon and an u-channel model diquark. Constraints on these models are obtained from the

(i) $t\bar{t}$ cross section measured at Tevatron.
(ii) AFB measured at Tevatron.
(iii) $t\bar{t}$ cross section measured at LHC with $\sqrt{s} = 7$ TeV.
(iv) AC measured at LHC with $\sqrt{s} = 7$ TeV.
(v) Resonance searches in the dijet channel at the LHC and
(vi) Resonance searches in the four-jets channel at the LHC.

The parameter space of the axigluon allowed within 2σ of the measured values of the stated observables includes a lower bound on the mass of the axigluon at 1.5 TeV with a corresponding coupling $\theta_A > 27°$. The allowed mass of the diquark is bounded from below by 300 GeV, and masses

above are allowed with the coupling of the model bounded from above by a value of 0.2 for smaller masses, which rises to $y_s < 2$ corresponding to $m_\phi = 3$ TeV. Another sliver of parameter space is allowed for larger couplings of the diquark due to destructive interference effects.

For the first time we have presented the complete density matrix of the top quark, including the off-diagonal elements for top-quark pair production processes in the axigluon and diquark models to aid further studies. We use these to show that the lepton polar asymmetry in the lab frame shows a correlation with the transverse polarization of the top quark for the axigluon model and even more significantly for the diquark model. The lepton asymmetry usually considered in studies of top polarization is calculated from lepton polar angle with respect to the top quark, and it does not show this correlation with transverse polarization. The correlation of transverse polarization with lepton azimuthal or energy asymmetry is also very small.

Finally, we extend our analysis to 13 TeV LHC, where, even though the values of the asymmetries get diluted, the correlations between accurate measurements of charge asymmetry and lepton asymmetries still separate out BSM and the SM in two-dimensional space. Taken together, these correlations can indeed be used to improve significance of the constraints on BSM from LHC data even in the initial stages of low luminosity.

ACKNOWLEDGMENTS

The authors are pleased to acknowledge conversations with Ritesh K. Singh, Arunprasath V, and Pratishruti Saha. R. M. G. wishes to acknowledge support from the Department of Science and Technology, India, under Grant No. SR/S2/JCB-64/2007. S. D. R. acknowledges support from the Department of Science and Technology, India, under Grant No. SR/SB/JCB-42/2009. The research of G. M. was supported by CSIR, India via SPM Grant No. 07/079(0095)/2011-EMR-I.

APPENDIX A: AC AT 13 TeV LHC

Since the AC calculated at NLO for 13 TeV LHC was unavailable at the time of submission of this work, we note that the available charge asymmetry values [48] form a smooth function of the beam energy and fit them to a polynomial to find the AC as a function of the beam energy. We obtain a fit to a polynomial presented in Eq. (A1) with goodness of fit parameter $r^2 = 0.9995$:

$$A_c(\sqrt{s}) = 3.12 \times 10^{-2} - 4.37 \times 10^{-3}\sqrt{s} + 2.6269 \times 10^{-4} s - 5.683 \times 10^{-6} s^{\frac{3}{2}}, \tag{A1}$$

This gives a value of $A_c(13\ \text{TeV}) = 0.0063$.

APPENDIX B: $t\bar{t}$ PRODUCTION DENSITY MATRICES

1. Axigluon density matrices

With $C_\theta = \cos(\theta_t)$, $S_\theta = \sin(\theta_t)$, $\beta = \sqrt{1 - \frac{4m_t^2}{\hat{s}}}$ and $\beta_A = \sqrt{1 - \frac{4m_t^2}{m_A^2}}$,

$$\rho^{++}_{bSM} = \frac{1}{{\Gamma_A}^2 {m_A}^2 + ({m_A}^2 - \hat{s})^2}\hat{s}^2\left\{\frac{1}{18}({g_A}^2 + {g_V}^2)(6 g_{\mathrm{At}} g_V \beta + 3 {g_{\mathrm{At}}}^2 \beta^2 - {g_V}^2(-4 + \beta^2)) + \frac{4}{9} g_A g_V (g_V + g^t_{\mathrm{A}}\beta)^2 C_\theta + \frac{1}{18}({g_A}^2 + {g_V}^2)\beta(2 g^t_{\mathrm{A}} g_V + {g^t_{\mathrm{A}}}^2\beta + {g_V}^2\beta) C_{2\theta}\right\}, \tag{B1}$$

$$\rho^{+-}_{bSM} = \frac{1}{{\Gamma_A}^2 {m_A}^2 + ({m_A}^2 - \hat{s})^2}\hat{s}^2\left(-\frac{8 g_A {g_V}^3 m_t S_\theta}{9\sqrt{\hat{s}}} - \frac{4 g^t_{\mathrm{A}} g_V ({g_A}^2 + {g_V}^2) m_t \beta C_\theta S_\theta}{9\sqrt{\hat{s}}}\right), \tag{B2}$$

$$\rho^{-+}_{bSM} = (\rho^{+-}_{bSM})^\star, \tag{B3}$$

$$\rho^{--}_{bSM} = \frac{1}{{\Gamma_A}^2 {m_A}^2 + ({m_A}^2 - \hat{s})^2}\hat{s}^2\left\{\frac{1}{18}({g_A}^2 + {g_V}^2)(-6 g^t_{\mathrm{A}} g_V \beta + 3 {g^t_{\mathrm{A}}}^2 \beta^2 - {g_V}^2(-4 + \beta^2)) - \frac{4}{9} g_A g_V (g_V - g_{\mathrm{A}}\beta)^2 C_\theta + \frac{1}{18}({g_A}^2 + {g_V}^2)\beta(-2 g^t_{\mathrm{A}} g_V + {g^t_{\mathrm{A}}}^2\beta + {g_V}^2\beta) C_{2\theta}\right\}, \tag{B4}$$

$$\rho^{++}_{\text{Inter ference}} = \frac{g_s^2}{9({\Gamma_A}^2 {m_A}^2 + ({m_A}^2 - \hat{s})^2)}\hat{s}(-{m_A}^2 + \hat{s}) \times (4 g_A (g_V + g^t_{\mathrm{A}}\beta) C_\theta + g_V(4 g_v + 3 g^t_{\mathrm{A}}\beta - g_V\beta^2 + \beta(g^t_{\mathrm{A}} + g_V\beta) C_{2\theta})), \tag{B5}$$

$$\rho^{+-}_{\text{Inter ference}} = \frac{g_s^2}{9({\Gamma_A}^2{m_A}^2 + ({m_A}^2 - \hat{s})^2)} 4m_t\sqrt{\hat{s}}S_\theta(g_A(2g_v({m_A}^2 - \hat{s}) + ig_{\text{At}}\Gamma_A m_A\beta) + g^t_{\text{A}}g_V({m_A}^2 - \hat{s})\beta C_\theta), \quad \text{(B6)}$$

$$\rho^{-+}_{\text{Interference}} = (\rho^{+-}_{\text{Interference}})^\star, \quad \text{(B7)}$$

$$\rho^{--}_{\text{Inter ference}} = \frac{g_s^2}{9({\Gamma_A}^2{m_A}^2 + ({m_A}^2 - \hat{s})^2)} ({m_A}^2 - \hat{s})\hat{s}(4g_A(g_V - g^t_{\text{A}}\beta)C_\theta + g_V(3g^t_{\text{A}}\beta + g_V(\beta^2 - 4) + \beta(g^t_{\text{A}} - g_V\beta)C_{2\theta})). \quad \text{(B8)}$$

To present the dependence on top boost and polar angle clearly, the amplitude square is written in terms of the polar angle θ in the $t\bar{t}$ center-of-momentum frame. The off-diagonal terms in the gluon-initiated process are zero, and the diagonal terms in the gluon-initiated process are not dependent on the top-quark polarization; therefore, we have omitted these here, and they can be found in many references, including Ref. [14]. The decay width of the axigluon at tree level is given by

$$\Gamma_A = \frac{4\pi}{6m_A}\{g_A^2(m_A^2(\beta_A + 5) - 4m_t^2\beta_A) + g_V^2(m_A^2(\beta_A + 5) + 2m_t^2\beta_A)\}. \quad \text{(B9)}$$

2. Diquark density matrices

The top-quark spin-density matrix for the u-channel exchange is given below in the $t\bar{t}$ center-of-momentum frame. The notation and SM-only contributions remain the same as for the case of the s-channel model.

$$\rho^{++}_{bSM} = \frac{2\hat{s}(y_P^2 + y_S^2)}{48(\beta\hat{s}C_\theta - 2m_t^2 + 2m_\phi^2 + \hat{s})^2}\{\hat{s}(2y_Py_S(\beta + \beta C_\theta^2 + 2C_\theta) + (y_P^2 + y_S^2)(2\beta C_\theta + C_\theta^2 + 1)) - 4C_\theta m_t^2(C_\theta(y_P^2 + y_S^2) + 2y_Py_S)\}, \quad \text{(B10)}$$

$$\rho^{+-}_{bSM} = -\frac{\hat{s}^{3/2}m_t y_P y_S(\beta C_\theta + 1)(y_P^2 + y_S^2)S_\theta}{6(\beta\hat{s}C_\theta - 2m_t^2 + 2m_\phi^2 + \hat{s})^2}, \quad \text{(B11)}$$

$$\rho^{-+}_{bSM} = (\rho^{+-}_{bSM})^\star, \quad \text{(B12)}$$

$$\rho^{--}_{bSM} = \frac{\hat{s}(y_P^2 + y_S^2)}{24(\beta\hat{s}C_\theta - 2m_t^2 + 2m_\phi^2 + \hat{s})^2}\{\hat{s}(-2y_Py_S(\beta + \beta C_\theta^2 + 2C_\theta) + (y_P^2 + y_S^2)(2\beta C_\theta + C_\theta^2 + 1)) - 4C_\theta m_t^2(C_\theta(y_P^2 + y_S^2) - 2y_Py_S)\}, \quad \text{(B13)}$$

$$\rho^{++}_{\text{Interference}} = \frac{g_s^2}{18(\beta\hat{s}C_\theta - 2m_t^2 + 2m_\phi^2 + \hat{s})} \times \{4(C_\theta^2 - 1)m_t^2(y_P^2 + y_S^2) - \hat{s}(2y_Py_S(\beta + \beta C_\theta^2 + 2C_\theta) + (y_P^2 + y_S^2)(2\beta C_\theta + C_\theta^2 + 1))\}, \quad \text{(B14)}$$

$$\rho^{+-}_{\text{Interference}} = \frac{g_s^2 2\sqrt{\hat{s}}m_t y_P S_\theta y_S(\beta C_\theta + 2)}{9(\beta\hat{s}C_\theta - 2m_t^2 + 2m_\phi^2 + \hat{s})},$$
$$\rho^{-+}_{\text{Interference}} = (\rho^{+-}_{\text{Interference}})^\star, \quad \text{(B15)}$$

$$\rho^{--}_{\text{Interference}} = \frac{g_s^2}{18(\beta\hat{s}C_\theta - 2m_t^2 + 2m_\phi^2 + \hat{s})} \times \{4(C_\theta^2 - 1)m_t^2(y_P^2 + y_S^2) - \hat{s}(-2y_Py_S(\beta + \beta C_\theta^2 + 2C_\theta) + (y_P^2 + y_S^2)(2\beta C_\theta + C_\theta^2 + 1))\}. \quad \text{(B16)}$$

[1] J. Lees *et al.* (*BABAR* Collaboration), Evidence of $B^+ \to \tau^+\nu$ decays with hadronic B tags, Phys. Rev. D **88**, 031102 (2013).

[2] CMS Collaboration, Report No. CMS-PAS-HIG-14-005.

[3] V. M. Abazov *et al.* (D0 Collaboration), Measurement of the Forward-Backward Asymmetry in the Production of $B^{\pm}$ Mesons in $p\bar{p}$ Collisions at $\sqrt{s} = 1.96$ TeV, Phys. Rev. Lett. **114**, 051803 (2015).

[4] S. Schael *et al.* (SLD Electroweak Group, DELPHI, ALEPH, SLD, SLD Heavy Flavour Group, OPAL, LEP Electroweak Working Group, L3 Collaboration), Precision electroweak measurements on the Z resonance, Phys. Rep. **427**, 257 (2006).

[5] C. W. Murphy, Bottom-quark forward-backward and charge asymmetries at hadron colliders, Phys. Rev. D **92**, 054003 (2015).

[6] V. Abazov *et al.* (D0 Collaboration), First Measurement of the Forward-Backward Charge Asymmetry in Top Quark Pair Production, Phys. Rev. Lett. **100**, 142002 (2008).

[7] T. Aaltonen *et al.* (CDF Collaboration), Forward-Backward Asymmetry in Top Quark Production in $p\bar{p}$ Collisions at $\sqrt{s} = 1.96$ TeV, Phys. Rev. Lett. **101**, 202001 (2008).

[8] V. M. Abazov *et al.* (D0 Collaboration), Measurement of the forward-backward asymmetry in top quark-antiquark production in $p\bar{p}$ collisions using the lepton + jets channel, Phys. Rev. D **90**, 072011 (2014).

[9] N. Kidonakis, Top quark forward-backward asymmetry at approximate N^3LO, Phys. Rev. D **91**, 071502 (2015).

[10] D. Choudhury, R. M. Godbole, R. K. Singh, and K. Wagh, Top production at the Tevatron/LHC and nonstandard, strongly interacting spin-one particles, Phys. Lett. B **657**, 69 (2007).

[11] O. Antunano, J. H. Kuhn, and G. Rodrigo, Top quarks, axigluons and charge asymmetries at hadron colliders, Phys. Rev. D **77**, 014003 (2008).

[12] P. Ferrario and G. Rodrigo, Constraining heavy colored resonances from top-antitop quark events, Phys. Rev. D **80**, 051701 (2009).

[13] P. H. Frampton, J. Shu, and K. Wang, Axigluon as possible explanation for $p\bar{p} \to t\bar{t}$ forward-backward asymmetry, Phys. Lett. B **683**, 294 (2010).

[14] D. Choudhury, R. M. Godbole, S. D. Rindani, and P. Saha, Top polarization, forward-backward asymmetry and new physics, Phys. Rev. D **84**, 014023 (2011).

[15] S. Dutta, A. Goyal, and M. Kumar, Top quark physics in the vector color-octet model, Phys. Rev. D **87**, 094016 (2013).

[16] S. Fajfer, J. F. Kamenik, and B. Melic, Discerning new physics in top-antitop production using top spin observables at hadron colliders, J. High Energy Phys. 08 (2012) 114.

[17] J. A. Aguilar-Saavedra and M. Perez-Victoria, Simple models for the top asymmetry: Constraints and predictions, J. High Energy Phys. 09 (2011) 097.

[18] M. Gresham, J. Shelton, and K. M. Zurek, Open windows for a light axigluon explanation of the top forward-backward asymmetry, J. High Energy Phys. 03 (2013) 008.

[19] S. Jung, H. Murayama, A. Pierce, and J. D. Wells, Top quark forward-backward asymmetry from new t-channel physics, Phys. Rev. D **81**, 015004 (2010).

[20] A. Papaefstathiou and K. Sakurai, Determining the helicity structure of third generation resonances, J. High Energy Phys. 06 (2012) 069.

[21] J. Shu, T. M. Tait, and K. Wang, Explorations of the top quark forward-backward asymmetry at the Tevatron, Phys. Rev. D **81**, 034012 (2010).

[22] V. Barger, W.-Y. Keung, and C.-T. Yu, Tevatron asymmetry of tops in a w′, z′ model, Phys. Lett. B **698**, 243 (2011).

[23] A. Rajaraman, Z. Surujon, and T. M. Tait, Asymmetric leptons for asymmetric tops, arXiv:1104.0947.

[24] K. M. Patel and P. Sharma, Forward-backward asymmetry in top quark production from light colored scalars in SO(10) model, J. High Energy Phys. 04 (2011) 085.

[25] E. L. Berger, Z. Sullivan, and H. Zhang, LHC and Tevatron constraints on a W' model interpretation of the top quark forward-backward asymmetry, Phys. Rev. D **88**, 114026 (2013).

[26] D.-W. Jung, P. Ko, J. S. Lee, and S.-h. Nam, Model independent analysis of the forward-backward asymmetry of top quark production at the Tevatron, Phys. Lett. B **691**, 238 (2010).

[27] D. Buarque Franzosi and C. Zhang, Probing the top-quark chromomagnetic dipole moment at next-to-leading order in QCD, Phys. Rev. D **91**, 114010 (2015).

[28] S. S. Biswal, S. Mitra, R. Santos, P. Sharma, R. K. Singh, and M. Won, New physics contributions to the forward-backward asymmetry at the Tevatron, Phys. Rev. D **86**, 014016 (2012).

[29] J. Shu, K. Wang, and G. Zhu, A revisit to top quark forward-backward asymmetry, Phys. Rev. D **85**, 034008 (2012).

[30] S. Westhoff, Top charge asymmetry—Theory status fall 2013, arXiv:1311.1127.

[31] M. Jezabek and J. H. Kuhn, Lepton spectra from heavy quark decay, Nucl. Phys. **B320**, 20 (1989).

[32] R. M. Godbole, S. D. Rindani, and R. K. Singh, Lepton distribution as a probe of new physics in production and decay of the t quark and its polarization, J. High Energy Phys. 12 (2006) 021.

[33] W. Bernreuther and Z.-G. Si, Distributions and correlations for top quark pair production and decay at the Tevatron and LHC., Nucl. Phys. **B837**, 90 (2010).

[34] J. Aguilar-Saavedra, W. Bernreuther, and Z. Si, Collider-independent top quark forward-backward asymmetries: Standard model predictions, Phys. Rev. D **86**, 115020 (2012).

[35] W. Bernreuther and Z.-G. Si, Top quark and leptonic charge asymmetries for the Tevatron and LHC, Phys. Rev. D **86**, 034026 (2012).

[36] J. Aguilar-Saavedra and R. Herrero-Hahn, Model-independent measurement of the top quark polarisation, Phys. Lett. B **718**, 983 (2013).

[37] J. L. Hewett, J. Shelton, M. Spannowsky, T. M. P. Tait, and M. Takeuchi, A^t_FB Meets LHC, Phys. Rev. D **84**, 054005 (2011).

[38] T. A. Aaltonen *et al.* (CDF, D0 collaborations), Combination of measurements of the top-quark pair production cross section from the Tevatron collider, Phys. Rev. D **89**, 072001 (2014).

[39] CMS Collaboration, Report No. CMS-PAS-TOP-12-003.

[40] ATLAS Collaboration, Report No. ATLAS-CONF-2012-134.
[41] N. Kidonakis and R. Vogt, The theoretical top quark cross section at the Tevatron and the LHC, Phys. Rev. D **78**, 074005 (2008).
[42] M. Czakon and A. Mitov, Top++: A program for the calculation of the top-pair cross-section at hadron colliders, Comput. Phys. Commun. **185**, 2930 (2014).
[43] M. Czakon, P. Fiedler, and A. Mitov, Total Top-Quark Pair-Production Cross-Section at Hadron Colliders Through $O(\alpha_S^4)$, Phys. Rev. Lett. **110**, 252004 (2013).
[44] V. Ahrens, A. Ferroglia, M. Neubert, B. D. Pecjak, and L. L. Yang, Top-pair forward-backward asymmetry beyond next-to-leading order, Phys. Rev. D **84**, 074004 (2011).
[45] T. Aaltonen *et al.* (CDF Collaboration), Measurement of the top quark forward-backward production asymmetry and its dependence on event kinematic properties, Phys. Rev. D **87**, 092002 (2013).
[46] M. Czakon, P. Fiedler, and A. Mitov, Resolving the Tevatron Top Quark Forward-Backward Asymmetry Puzzle, Phys. Rev. Lett. **115**, 052001 (2015).
[47] ATLAS, CMS Collaborations, Report No. ATLAS-CONF-2014-012.
[48] J. H. Kuhn and G. Rodrigo, Charge asymmetries of top quarks at hadron colliders revisited, J. High Energy Phys. 01 (2012) 063.
[49] T. A. Aaltonen *et al.* (CDF Collaboration), Measurement of the leptonic asymmetry in $t\bar{t}$ events produced in $p\bar{p}$ collisions at $\sqrt{s} = 1.96$ Tev, Phys. Rev. D **88**, 072003 (2013).
[50] V. M. Abazov *et al.* (D0 Collaboration), Measurement of the forward-backward asymmetry in the distribution of leptons in $t\bar{t}$ events in the lepton + jets channel, Phys. Rev. D **90**, 072001 (2014).
[51] T. Aaltonen *et al.* (CDF Collaboration), Measurement of $t\bar{t}$ spin correlation in $p\bar{p}$ collisions using the CDF II detector at the Tevatron, Phys. Rev. D **83**, 031104 (2011).
[52] Y. Peters (D0 Collaboration), $t\bar{t}$ spin correlations at D0, *Proc. Sci.*, ICHEP2012 (2013) 236.
[53] G. Aad *et al.* (ATLAS Collaboration), Measurements of spin correlation in top-antitop quark events from proton-proton collisions at $\sqrt{s} = 7$ TeV using the ATLAS detector, Phys. Rev. D **90**, 112016 (2014).
[54] S. Chatrchyan *et al.* (CMS Collaboration), Measurements of $t\bar{t}$ Spin Correlations and Top-Quark Polarization Using Dilepton Final States in pp Collisions at $\sqrt{s} = 7$ TeV, Phys. Rev. Lett. **112**, 182001 (2014).
[55] S. Frixione and B. R. Webber, Matching NLO QCD computations and parton shower simulations, J. High Energy Phys. 06 (2002) 029.
[56] G. Aad *et al.* (ATLAS Collaboration), Measurement of Top Quark Polarization in Top-Antitop Events from Proton-Proton Collisions at $\sqrt{s} = 7$ TeV Using the ATLAS Detector, Phys. Rev. Lett. **111**, 232002 (2013).
[57] P. H. Frampton and S. L. Glashow, Chiral color: An alternative to the standard model, Phys. Lett. B **190**, 157 (1987).
[58] P. Frampton, Chiral Dilepton Model and the Flavor Question, Phys. Rev. Lett. **69**, 2889 (1992).
[59] J. Pumplin, D. Stump, J. Huston, H. Lai, P. M. Nadolsky, and W.-K. Tung, New generation of parton distributions with uncertainties from global QCD analysis, J. High Energy Phys. 07 (2002) 012.
[60] V. Khachatryan *et al.* (CMS Collaboration), Search for resonances and quantum black holes using dijet mass spectra in proton-proton collisions at $\sqrt{s} = 8$ TeV, Phys. Rev. D **91**, 052009 (2015).
[61] J. Aguilar-Saavedra, Portrait of a colour octet, J. High Energy Phys. 08 (2014) 172.
[62] R. S. Chivukula, E. H. Simmons, and C.-P. Yuan, Axigluons cannot explain the observed top quark forward-backward asymmetry, Phys. Rev. D **82**, 094009 (2010).
[63] CMS Collaboration, Report No. CMS-PAS-B2G-12-008.
[64] S. Chatrchyan *et al.* (CMS Collaboration), Search for Pair-Produced Dijet Resonances in Four-Jet Final States in pp Collisions at $\sqrt{s} = 7$ TeV, Phys. Rev. Lett. **110**, 141802 (2013).
[65] M. I. Gresham, I.-W. Kim, S. Tulin, and K. M. Zurek, Confronting top AFB with parity violation constraints, Phys. Rev. D **86**, 034029 (2012).
[66] B. Grinstein, A. L. Kagan, M. Trott, and J. Zupan, Forward-Backward Asymmetry in $t\bar{t}$ Production from Flavour Symmetries, Phys. Rev. Lett. **107**, 012002 (2011).
[67] B. Diaz and A. R. Zerwekh, Axigluon phenomenology using ATLAS dijet data, Int. J. Mod. Phys. A **28**, 1350133 (2013).
[68] D. Choudhury, R. M. Godbole, and P. Saha, Dijet resonances, widths and all that, J. High Energy Phys. 01 (2012) 155.
[69] K. Melnikov and M. Schulze, NLO QCD corrections to top quark pair production and decay at hadron colliders, J. High Energy Phys. 08 (2009) 049.
[70] W. Bernreuther, P. Gonzalez, and C. Mellein, Decays of polarized top quarks to lepton, neutrino and jets at NLO QCD, Eur. Phys. J. C **74**, 2815 (2014).
[71] E. L. Berger, Q.-H. Cao, C.-R. Chen, and H. Zhang, Interpretations and implications of the top quark rapidity asymmetries a_{FB}^t and $a_{\mathrm{FB}}^{E_l}$, Phys. Rev. D **88**, 014033 (2013).
[72] E. L. Berger, Q.-H. Cao, J.-H. Yu, and H. Zhang, Measuring top-quark polarization in top-pair + missing energy events, arXiv:1305.7266.
[73] R. M. Godbole, K. Rao, S. D. Rindani, and R. K. Singh, On measurement of top polarization as a probe of $t\bar{t}$ production mechanisms at the LHC, J. High Energy Phys. 11 (2010) 144.
[74] R. M. Godbole, L. Hartgring, I. Niessen, and C. D. White, Top polarisation studies in $h^- t$ and wt production, J. High Energy Phys. 01 (2012) 011.
[75] V. Barger, W.-Y. Keung, and B. Yencho, Azimuthal correlations in top pair decays and the effects of new heavy scalars, Phys. Rev. D **85**, 034016 (2012).
[76] M. Baumgart and B. Tweedie, A new twist on top quark spin correlations, J. High Energy Phys. 03 (2013) 117.
[77] F. Boudjema and R. K. Singh, A model independent spin analysis of fundamental particles using azimuthal asymmetries, J. High Energy Phys. 07 (2009) 028.
[78] J. Shelton, Polarized tops from new physics: Signals and observables, Phys. Rev. D **79**, 014032 (2009).
[79] A. Carmona, M. Chala, A. Falkowski, S. Khatibi, M. M. Najafabadi, G. Perez, and J. Santiago, From Tevatron's top and lepton-based asymmetries to the LHC, J. High Energy Phys. 07 (2014) 005.

[80] A. Prasath, R. M. Godbole, and S. D. Rindani, Longitudinal top polarisation measurement and anomalous Wtb coupling, Eur. Phys. J. C **75**, 402 (2015).

[81] J. Drobnak, J. F. Kamenik, and J. Zupan, Flipping $t\bar{t}$ Asymmetries at the Tevatron and the LHC, Phys. Rev. D **86**, 054022 (2012).

[82] W. Bernreuther, A. Brandenburg, and P. Uwer, Transverse polarization of top quark pairs at the Tevatron and the Large Hadron Collider, Phys. Lett. B **368**, 153 (1996).

[83] J. Aguilar-Saavedra, Quantum coherence, top transverse polarisation and the Tevatron asymmetry A_{FB}^{l}, Phys. Lett. B **736**, 132 (2014).

[84] M. Baumgart and B. Tweedie, Transverse top quark polarization and the $t\bar{t}$ forward-backward asymmetry, J. High Energy Phys. 08 (2013) 072.

[85] D. Krohn, T. Liu, J. Shelton, and L.-T. Wang, A polarized view of the top asymmetry, Phys. Rev. D **84**, 074034 (2011).